A 28-GHz Inverse Class-F Power Amplifier with Coupled-Inductor based Harmonic Impedance Modulator

Seyed Yahya Mortazavi and Kwang-Jin Koh

Multifunctional Integrated Circuits and Systems Group, Virginia Tech, Blacksburg, USA

***Abstract* — This paper presents a 28 GHz class-F^{-1} power amplifier in 0.13-µm SiGe BiCMOS technology. The PA adopts a coupled-inductor based harmonic impedance modulator in order to terminate 2nd and 3rd harmonic load impedances appropriately for class-F^{-1} operation. The coupled coils essentially provide frequency-dependent inductance that is optimal to resonate out 2nd and 3rd harmonic reactive impedance. The PA achieve 40-42% PAE over 27.5 GHz to 29 GHz, peak 42% PAE at 28 GHz with 50 mW OP_{-1dB} power, one of the highest PAEs ever reported in silicon-based PAs. At 6-dB backoff output power, the PAE is as high as 20%. P_{sat} is 16.6 dBm. The PA occupies 0.55×0.96 mm².**

***Index Terms* — Class-AB, class-F, inverse class-F, millimeter wave, power amplifier, SiGe, 28 GHz, 38 GHz, 5 G LTE.**

I. Introduction

Millimeter (mm) wave communication at 28 GHz and 38 GHz has been gaining growing attention for next-generation 5G cellular networks to accommodate explosive demands on higher data-rate in wireless communications. Directional antennas and beamforming arrays prove to be essential for a maximum channel capacity at these frequency bands for both base stations and mobile devices [1]. Design of high power-added-efficiency (PAE) power amplifiers (PAs) with output power level of 15~17 dBm, as a main building block, is critical for the uplink multi-element beamformers [2]. In recently proposed high-efficiency silicon PAs [3]-[6], harmonic loads are tuned to make a non-overlapping voltage and current waveform at power device to reduce DC power dissipation. This paper proposes a new coupled-inductor based harmonic impedance modulator that provides frequency-dependent inductance to optimally terminate 2nd and 3rd harmonic impedances for class-F^{-1} operation. The proposed 2-stage class-F^{-1} PA employing proposed load network achieves 42% peak PAE with 50 mW P_{out} and 21 dB gain at 28 GHz.

II. Coupled Inductor: Impedance Modulator

In the coupled inductors shown in Fig. 1, effective inductances of the primary and secondary inductors depend on the mutual inductance M, and the magnitude (A) and phase (ϕ) of the current ratio i_2/i_1. If the primary and secondary currents are in phase (ϕ=0), their magnetic flux will be additive, effectively increasing inductances of both primary, L_{eff1}, and secondary, L_{eff2}, and therefore enhancing quality factor of the inductors. However, the induction of

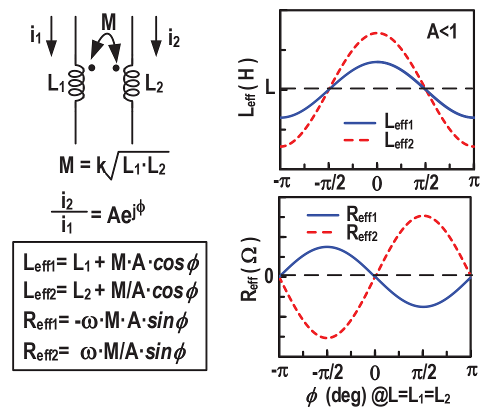

Fig. 1. Impedance modulation in the coupled inductors.

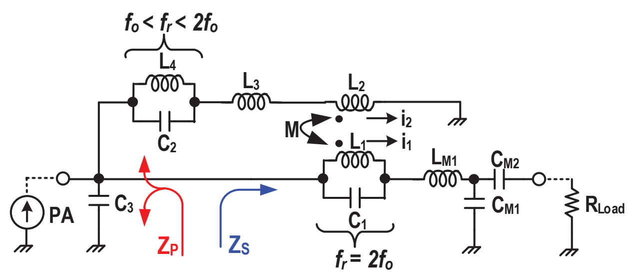

Fig. 2. Proposed inverse class-F load with coupled inductors.

out-of-phased currents (ϕ=±π) between the coupled coils diminishes magnetic flux linkage, reducing the inductance of the coils. In general excitation of arbitrary phase currents in the coupled coils, *in-phase* current component alters the mutual flux, modulating mutual inductance, whereas *quadrature* component modifies effective coil resistance. Therefore, the impedance of the coupled inductor can be modulated dramatically by controlling A and ϕ; when $|\phi|=\pi$, L_{eff} becomes even negative (or capacitive) at primary ($A > L_1/M$) or secondary ($A < M/L_2$) depending on A. For a perfect orthogonal case ($\phi=\pm\pi/2$), the magnetic coupling will not happen but energy exchanges between the primary and secondary inductors, as evidenced by the negative resistance in the primary ($\phi=-\pi/2$) or secondary ($\phi=\pi/2$) inductor in Fig. 1.

III. Class-F^{-1} Load with Coupled Inductor

Fig. 2 shows proposed load network employing coupled coils for class F^{-1} PA that modulates the load impedance optimally at different frequency bands by controlling A and ϕ of the coupled inductors to provide an optimum load at

978-1-4799-8682-8/15/$31.00 ©2015 IEEE

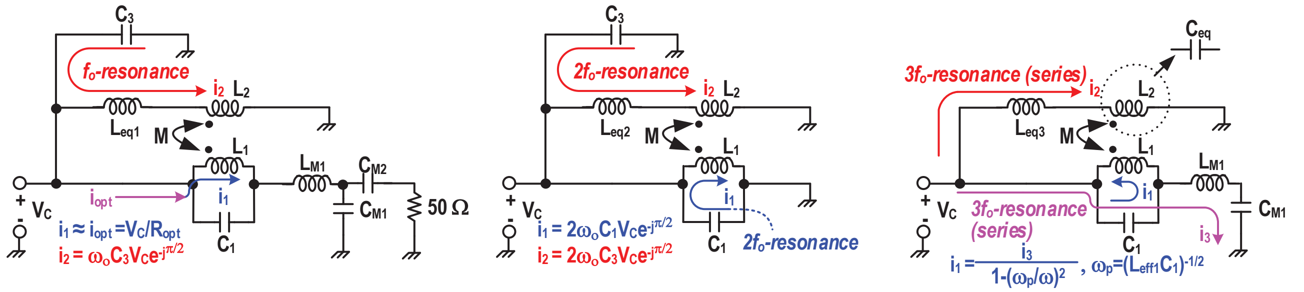

(a) (b) (c)

Fig. 3. Equivalent load network: (a) at f_o (signal) band, (b) at $2f_0$ (second harmonic) band, and (c) at $3f_0$ (third harmonic) band.

signal band, a high impedance at 2nd harmonic band, and a low impedance at 3rd harmonic band. The load network comprised of a parallel of Z_S, the impedance of series signal path to the 50-Ω output load, and Z_P, the impedance of parallel path which includes total parasitic capacitance (C_3) at the collector node of a PA. By coupling the two inductors L_1 and L_2, the series and parallel loads become dependent on each other, enabling *a coupled-loop impedance control* by the coupled coils that essentially provides *frequency dependent inductance* at both primary and secondary paths.

Z-modulation @ f_o-band: Fig. 3(a) shows the equivalent load network at signal band (f_0) where the $2f_o$ resonator (L_1-C_1) can be approximated to L_1. Likewise, the series of L_4-C_2 resonator ($f_o<f_r<2f_o$) and L_3 in Fig. 2 can be replaced with its equivalent inductance L_{eq1}. The series network matches the 50-Ω load to an optimum load so that the optimum current, i_{opt} ($=V_C/R_{opt}$), flowing to the series network is in-phase with the collector voltage, V_C. Most of the optimum curent flows to the primary inductor, $i_1 \approx i_{opt}$, which is in-phase with the V_C as well. In the parallel path the series inductance of $L_{eq1}+L_{eff2}$ resonates out C_3 and provides a high impedance at the f_o-band. Thus, the current flowing to the secondary inductor lags V_C by $\pi/2$, resulting in $\phi=-\pi/2$. Therefore, no coupling will happen at the signal band and effective inductance at the primary and secondary does not change. $\phi=-\pi/2$ will introduce a positive resistance of R_{eff1} ($=\omega_o M\cdot A$ in Fig. 1) in the L_1, causing a power loss. This, however, will not degrade the efficiency since the secondary negative resistance ($R_{eff2}=-\omega_o M/A$ in Fig. 1) will feed the power back to the signal path. CAD simulation confirms that there is no power loss from collector node to the 50-Ω load and no stability issue arises.

Z-modulation @$2f_o$-band: The equivalent load network at $2f_0$-band is shown in Fig. 3(b). In the series path, L_{eff1} resonates C_1 at $2f_0$ and provides a high impedance and almost all voltage drops on the resonator. Therefore, the series load is simplified with L_1-C_1. In the parallel load, the L_4-C_2 resonator in Fig. 2 becomes a capacitor equivalently at the $2f_0$-band after passing its resonance. This capacitor in series with L_3 in Fig. 2 forms an equivalent inductor L_{eq2}

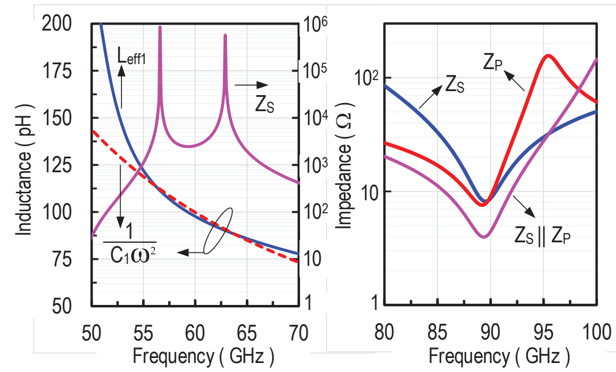

(a) (b)

Fig. 4. (a) Effective inductance (L_{eff1}) and required inductance $[1/(C_1\omega^2]$ for $2f_0$-resonance, and resonant tank impedance (Z_S), (b) series (Z_S), parallel (Z_P) and total impedance ($Z_S \parallel Z_P$) at $3f_0$-band.

that resonates out C_3, thus making a high parallel impedance at $2f_o$-band as well. Therefore, the i_1 and i_2 are in phase. Since $\phi=0$, both L_{eff1} and L_{eff2} are higher than their self-inductances, enhancing the quality factor of the inductors. In Fig. 4(a) $1/C_1\omega^2$ is the required inductance to resonate out C_1 at $2f_0$-band. As frequency increases A becomes smaller, decreasing L_{eff1} and resulting in a frequency-dependent inductance that perfectly follows the required inductance at the target $2f_o$-band for resonance. This achieves very large impedance ($Z_S > 1$ kΩ in Fig. 4(a)) all over the 2nd harmonic band in the series path, suitable for Class-F^{-1} operation.

Z-modulation @$3f_o$-band: In the equivalent load circuit at $3f_0$-band shown in Fig. 3(c), L_{M1} and C_{M1} are optimized to make a series resonance with an equivalent capacitance from the L_1-C_1 resonator at the 3rd harmonic band. The circulating current, i_1, in the LC tank induces out-of-phase coupled current of i_2 in the secondary inductor. Due to the frequency dependency of L_{eff1} the ω_p in Fig. 3 can be close to the 3rd harmonic frequency, decreasing $A=|i_2/i_1|$ to much smaller than 1. Therefore, the secondary inductor becomes negative inductance (or capacitance) and can resonate L_{eq3} at $3f_o$-band. Thus, both series and parallel paths make series resonance, shorting the collector node to ground and thereby terminating the 3rd harmonic impedance more

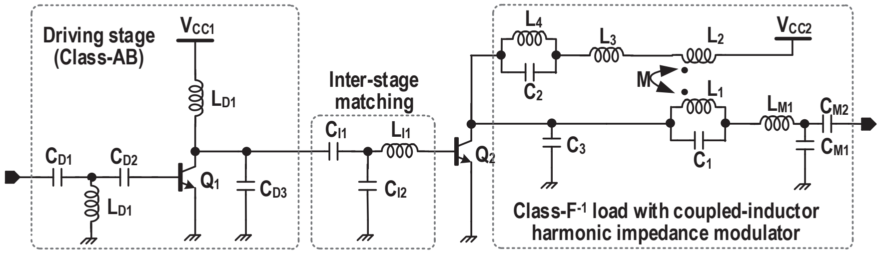

Fig. 5. 2-stage PA: cascade of class-AB driver with class-F^{-1} output power stage employing proposed coupled-inductor harmonic impedance modulator.

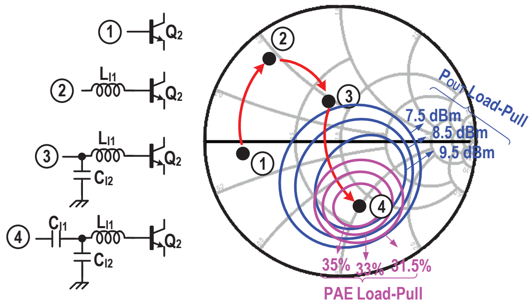

Fig. 6. Load-pull design of the inter-stage matching network.

effectively. The impedance simulation results at the $3f_0$-band shown in Fig. 4(b) confirm the operation: after the series resonance, each path (Z_P & Z_S) provides ~8 Ω due to finite resonator Q at ~90 GHz. The overall impedance, however, becomes half because of the dual paths resonance.

IV. Power Amplifier Design

Fig. 5 shows schematic of the proposed 2-satge PA, cascade of class-AB driver and class-F^{-1} power stage, adopting proposed coupled inductor load network at the output stage. In the driver, the T-network composed of T-line inductor L_{D1} (180 pH) and MIM capacitors, C_{D1} (93f fF) and C_{D2} (143 fF) matches input to 50 Ω over 27-31 GHz. The size and class-AB bias point of Q_1 (l_e=16 µm) and V_{CC1} (2 V) are optimally chosen to drive the output stage into saturation when the driver output power is near 1-dB compression point (9 dBm). As seen in Fig. 6, load-pull simulations reveal that optimum inter-stage impedance for > 9 dBm driver output power with > 35% driver PAE is capacitive (34-j51 Ω). Therefore, L_{D1} (220 pH) resonates out only a portion of C_{D3} to provide the optimum capacitive impedance. A step-by-step approach to match a low input impedance of Q_2 to the optimum inter-stage impedance is illustrated in Fig. 6. Design values are L_{I1}=145 pH, C_{I1}=67 fF, and C_{I2}=153 fF.

In the output stage, Q_2 is sized (l_e = 2×13 µm) to have a peak f_T current density (1.4 mA/µm) at the 15 dBm of output 1-dB compression point, allowing maximum PAE at the output power level. Fig. 7 shows the coupled inductor layout implemented using top metal layer, where the

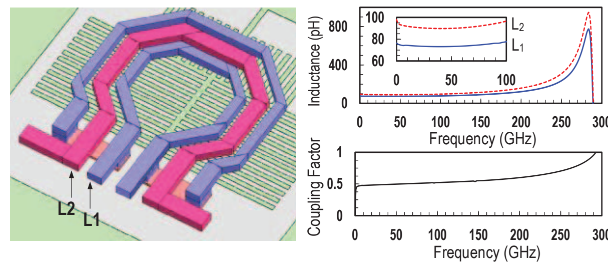

Fig. 7. Coupled inductor layout and EM-simulation results

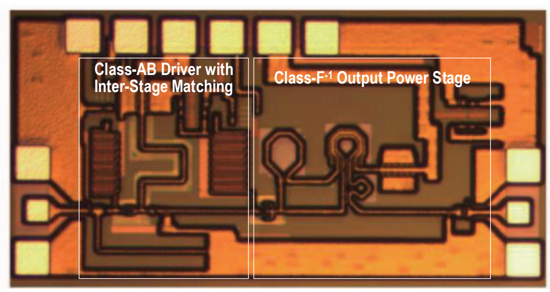

Fig. 8. Chip photograph (size: 0.55×0.96 mm^2).

secondary inductor (L_2) is enclosed by the primary inductor (L_1). This gives ~0.5 of coupling factor in EM simulations (Sonnet Software). L_1 (70 pH) and L_2 (90 pH) are fairly constant over 150 GHz and self-resonance frequency is greater than 250 GHz. Magnetic coupling allows the primary inductor L_1 to be variable from 120 pH to 80 pH over the increase of frequency at $2f_o$-band (54-61 GHz). This enables a *frequency-tracking* resonance in the primary path, resulting in a high impedance over the entire $2f_o$-band as discussed. Added benefit by the mutual coupling is the Q enhancement in the range of 1.2~1.8 times in the coupled inductors at the $2f_o$-band in simulations.

V. Measurement Results

Fig. 8 shows chip photograph fabricated in IBM8HP 0.13 µm SiGe BiCMOS process (f_T/f_{max}=180/220 GHz). Die size including pads is 0.55×0.96 mm^2. On-wafer small-signal S-parameter measurement is performed after SOLT calibration. Fig. 9 shows the measurement and simulation results at a class AB bias point (V_{CC1}/V_{CC2}=2/2.4 V, I_{CC1}/I_{CC2}=3/10 mA): S_{11}<-10 dB, S_{22}<-8 dB and S_{21}=18-21.5 dB over 27-31 GHz. The PA is stable over all frequencies. For large signal measurements, the input and

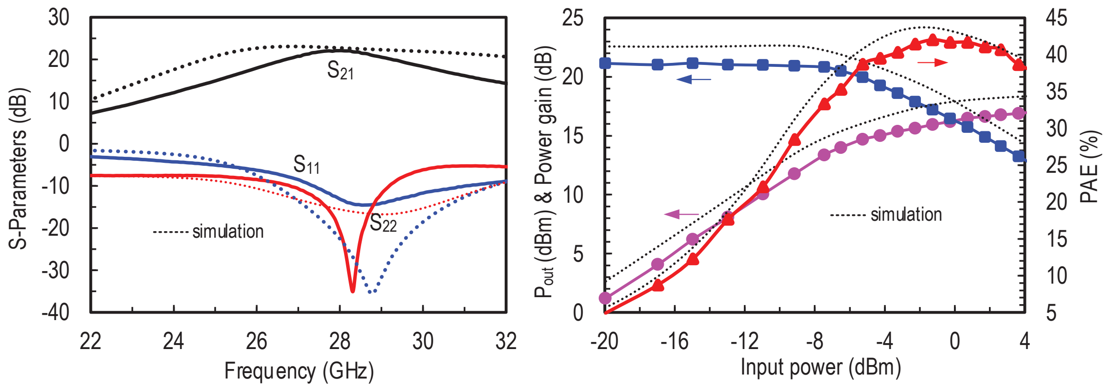

(a) (b)

Fig. 9. Measured PA performance: (a) S-parameters and (b) P_{out}, power gain (S_{21}), and PAE versus input power.

Table I: Performance comparison with state-of-the-art silicon-based PAs at microwave and mm-wave frequencies

Authors	Freq.(GHz)	PAE (%)	P_{sat} (dBm)	OP_{-1dB}(dBm)	Gain (dB)	Size (mm^2)	Supply (V)	Technology	Feature
This Work	**27-31**	**37-42%**	**17.1**	**15**	**21.2**	**0.49**	**2.4**	**0.13μm SiGe**	**2-stage Class-F^{-1}**
ISSCC 2014 SY. Mortazavi *et al.*	28	40.7	17.1	15	10.3	0.27	2.2	0.13μm SiGe	1-stage Class-F^{-1}
SiRF 2014 A. Sarkar *et al.*	28	35.3	18.6	15.5	15.3	0.43	3.6	0.13μm SiGe	2-stage Class-J
RFIC 2015 SY. Mortazavi *et al.*	38	38.5	17.2	15.5	16.5	0.5	2.3	0.13μm SiGe	2-stage Class-F^{-1}
BCTM 2011 H. Dabag *et al.*	37.5	26.2	14.8	NA	11.5	0.27	2.4	0.13μm SiGe	2-Stage Class-B
JSSC 2014 K. Datta *et al.*	41	36	18.1	NA	5.6	0.74	2.5	0.13μm SiGe	1-stage Class-E
RFIC 2012 A. Agah *et al.*	42.5	34.4	18.6	17.5	9.5	0.3	2.7	45nm SOI CMOS	3-stack Class-AB
RFIC 2014 J-H. Chen *et al.*	18	41.4	15.9	13.3	11	0.62	2	45nm SOI CMOS	Cascode Class-E

output powers of PA are measured using R&S power sensors (NRP-Z57) and power meter built in a spectrum analyzer (FSU43). RF cable loss (typically ~1.8 dB) is characterized and de-embedded carefully over the operational frequency range. The PA achieves 37~42% PAE at 27-31 GHz and the PAE is higher than 40% from 27.5 GHz to 29 GHz. Fig. 9 (b) shows large signal power measurement results at 28 GHz. The PA reaches to peak 42% PAE with 15 dBm P_{out} at 28GHz. At 6-dB back-off output power the measured PAE is as high as 20%. The measured P_{sat} is 16.5 dBm and output P_{-1dB} point is 15 dBm. Table I compares the performance of the PA with state-of-the-art silicon-based power amplifiers. This work achieves one of the highest PAE reported so far at microwave and mm-wave frequencies.

VI. Conclusion

This paper presents class-F^{-1} power amplifier implemented in 0.13-µm SiGe BiCMOS process. In the PA, a coupled-inductor based harmonic impedance modulator terminates 2^{nd} and 3^{rd} harmonic impedances appropriately for optimal class-F^{-1} operation, achieving 42 % peak PAE at 28 GHz with 50 mW P_{out}. The coupled inductors can be integrated compactly at mm-wave, claiming no particular area penalty but providing powerful harmonic impedance control, promising for a high efficiency at mm-wave.

Acknowledgement

The authors would like to thank Lockheed Martin for the silicon chip fabrication and Rohde & Schwartz for their help in the measurement equipment.

References

[1] T.S. Rappaport, et al, "Millimeter Wave Mobile Communications for 5G Cellular: It Will Work!," IEEE Access, vol.1, pp.335-349, 2013.

[2] A. Sarkar, et al, "A power-efficient 4-element beamformer in 120-nm SiGe BiCMOS for 28-GHz cellular communications," 2014 IEEE BCTM, pp.68-71, Sept. 2014.

[3] S. Y. Mortazavi, et al, "A Class F^{-1}/F 24-to-31GHz power amplifier with 40.7% peak PAE, 15dBm OP1dB, and 50mW Psat in 0.13µm SiGe," *IEEE ISSCC*, pp.254-255, Feb. 2014.

[4] A. Sarkar and, et al, "A 28-GHz class-J Power Amplifier with 18-dBm output power and 35% peak PAE in 120-nm SiGe BiCMOS," *IEEE SiRF,* pp.71-73, Jan. 2014.

[5] S. Y. Mortazavi, et al, " A 38 GHz Inverse Class-F Power Amplifier with 38.5% Peak PAE, 16.5 dB Gain, and 50 mW Psat in 0.13-µm SiGe BiCMOS," *IEEE RFIC*, May 2015.

[6] K. Datta, et al, "Performance Limits, Design and Implementation of mm-Wave SiGe HBT Class-E and Stacked Class-E Power Amplifiers," *IEEE JSSC*, vol.49, no.10, pp.2150-2171, Oct. 2014.